

SAR Focusing Performance for Moving Objects with Random Motion Components

Ahmed R. Fasih, Emre Ertin, Joshua N. Ash, Randolph L. Moses
 The Ohio State University
 Department of Electrical and Computer Engineering
 2015 Neil Avenue, Columbus, OH 43220

Abstract—Synthetic aperture radar imaging is generally based on the assumption that objects in the scene are stationary. Many approaches have been proposed that compensate for a moving target when one wishes to track or image it. In this paper we consider moving objects that have random fluctuations in their motion, for example caused by engine vibration or road jitter. We study the Cramér-Rao bounds for estimating the location and velocity of a scattering center on such a target, and show that with even small random fluctuations, achievable focusing performance can be several times worse than for a stationary object.

I. INTRODUCTION

A synthetic aperture radar (SAR) image represents the concentration of electromagnetic energy reflected by objects in the illuminated scene. As radar has all-weather, day-night, persistent sensing capabilities and range-independent resolution, many uses have been found for *airborne* SAR platforms that circle a ground scene of interest.

Traditional SAR imaging algorithms require a fully stationary scene to produce an ideal image. In urban environments, moving targets are inevitable and they introduce significant artifacts into a SAR image: for example, constant velocity can shift target signatures or severely defocus them, or both. There is interest in obtaining unartifacts images of moving targets (or simply tracking them). Moving target focusing algorithms that have been proposed make some assumption about target motion, for example constant velocity [1], [2], or low-order polynomial motion [3], [4].

This present work seeks to extend the theoretical bounds on stationary point scatterer focusing [5] by considering *non-zero velocity* as well as *random* target motion. This is motivated by the observation that all targets move with some random component. These random contributions to target motion may come from road jitter, engine vibrations, etc., and are not well-represented by low-order polynomial models, so are not amenable to moving target focusing.

Our goal is a theoretical lower bound on the location estimation accuracy of scattering centers when their motion is characterized by constant velocity movement perturbed by random motion. We arrive at this bound by computing the Cramér-Rao bound (CRB) for estimating a scatterer’s amplitude, position, and velocity (the analysis extends to acceleration and higher orders of motion). In this paper, we first briefly introduce SAR imaging and notation. Then

two methods for obtaining the CRB is described: a linear-approximation analytical approach and a numerical Monte Carlo solution. A number of computational experiments that quantify the achievable focusing accuracy of targets moving with random components will be presented.

II. MATHEMATICAL DESCRIPTION OF SAR

Synthetic aperture radar imaging involves an airborne antenna that broadcasts a uniquely-shaped electromagnetic pulse at the ground, and “listens” for echoes reflected by targets in the scene. This transmit-receive pattern is repeated as the aircraft flies past a scene, and it is this diversity of viewing angles that allows several one-dimensional range returns to be combined into a two-dimensional image of reflector location and response amplitude.

If the radar pulse broadcast is a linear chirp with center frequency f_c and bandwidth B , the data vector sampled at time $t \in [-T_0, T_0]$ is given by

$$\vec{Z}(t) = \sum_{i=1}^N a_i \exp(j \underbrace{\frac{4\pi}{c} \vec{f} \hat{p}(t)^T \vec{R}_i(t)}_{\vec{\Phi}_i(t)}) + \vec{n}_Z(t), \quad (1)$$

where the scene is modeled a collection of N point scatterers, each with its own complex amplitude $a_i = |a_i| e^{j\angle a_i}$, and three-dimensional location $R_i(t) = [x_i(t), y_i(t), z_i(t)]^T$. Here, \vec{f} is the $N_f \times 1$ vector of broadcast frequencies, $f_n \in [f_c - \frac{B}{2}, f_c + \frac{B}{2}]$, $n = 1, \dots, N_f$, and $\hat{p}(t) = [\sin \phi_t \cos \theta_t, \cos \phi_t \cos \theta_t, \sin \theta_t]^T$ is a unit vector that points from the scene center to the aircraft at time t . The x axis is parallel to the flightpath at $t = 0$, the y -axis points away from the platform at $t = 0$ and the z -axis point upward. This model assumes azimuth and elevation angles ϕ_t and θ_t respectively, which describe the orientation of the radar with respect to the scene. The origin is the scene’s center. This model is standard and detailed in, e.g., [6].

The phase vector, $\vec{\Phi}(t)$, links this standard SAR model to echo-based range-finding. This $N_f \times 1$ vector simply encodes *the number of radian wavelengths between the radar and the scatterer* for each frequency in the broadcasted chirp. The distance between the scene center and the i th scatterer is encoded by the inner product $\hat{p}(t)^T \vec{R}_i(t)$. Then, $2\pi \cdot 2 \frac{f_n}{c} \hat{p}(t)^T \vec{R}_i(t)$ is the round-trip number of wavelengths for frequency f_n in radians (since the distance between the radar and the scene center can be assumed to be known).

Let the number of pulses broadcast be N_ϕ , giving $N_f \cdot N_\phi$ total data points collected over an imaging interval. This observed phase history measurement is corrupted by complex additive white Gaussian sensor noise with variance σ_n^2 . Once collected and properly formatted, this phase history is converted to an image using the two-dimensional FFT or filtered backprojection [6]. Rigling provides a detailed study of imaging artifacts under deterministic motion [7].

We next consider the Cramér-Rao bound of a single point scatterer with both constant velocity and random motion components.

III. FOCUSING PERFORMANCE BOUNDS FOR A SINGLE SCATTERER

Consider a single point scatterer with position

$$\vec{R}(t) = \begin{bmatrix} x_0 + v_x t + W_x(t) \\ y_0 + v_y t + W_y(t) \\ z_0 + v_z t + W_z(t) \end{bmatrix} \quad (2)$$

with nominal position x_0, y_0, z_0 , three-dimensional velocity v_x, v_y, v_z , and three colored Gaussian random noise processes that represent deviations from ideal constant-velocity motion, $W_x(t), W_y(t)$, and $W_z(t)$.

The Cramér-Rao bound provides a lower bound on the mean-squared error of any unbiased estimator, $\hat{\theta}$, of a deterministic unknown parameter vector, Θ , from data \underline{Z} . Assuming $\hat{\theta}$ is an unbiased estimator,

$$\text{MSE}(\hat{\theta}) \geq P_{CR} = F^{-1} \quad (3)$$

where F , the Fisher information matrix (FIM), is given by

$$F = -E_{\underline{Z}}[\partial_{\Theta} \partial_{\Theta}^T \log P(\underline{Z}|\Theta)], \quad (4)$$

where $\partial_a \equiv \frac{\partial}{\partial a}$. That is, the CRB matrix P_{CR} is the inverse of the Fisher information matrix, which is a function of the probability of the observed data.

Returning to the SAR data model, the observed data's phase $\vec{\Phi}(t) = \frac{4\pi f}{c} \hat{p}(t)^T \vec{R}(t)$ is a linear combination of Gaussian random variables and therefore is itself a Gaussian random vector. However, the joint distribution of $\exp(j\vec{\Phi}(t))$ is not a standard distribution. A small extension of [8, pp. 520-522] gives the joint distribution of the *magnitude and angle* of a single sinusoidal random variable, $\exp(j\psi) + n$, where ψ and n are normally-distributed with arbitrary mean and variance. However, it involves numerically integrating out the random phase ψ , and does not seem to scale well for vector-valued signals.

Inspired by this approach, we consider the *real and imaginary components* of $\vec{Z}(t)$ and show that it is quite easy to obtain the joint distribution of these two random vectors numerically. When the random motion components $W_x(t), W_y(t), W_z(t)$ are uncorrelated over time, the joint density over *all* data samples simplifies into a product of likelihoods, each involving just one numerical integration.

We describe two ways to compute the bound, and then apply them to understand focusing performance under varying operating parameters.

Below, we describe two ways to compute the Cramér-Rao bound for jointly estimating scatterer amplitude, position, and

velocity. First, we develop a CRB expression by sampling log-likelihood values, and second, we consider a simpler (but less accurate) method based on analysis of a linearized data model.

A. Sampling the complete CRB

The real and imaginary components of observation vector $\vec{Z}(t)$, given the random motion $\vec{W}(t) = [W_x(t), W_y(t), W_z(t)]^T$, are multivariate-normal:

$$\begin{bmatrix} \Re \vec{Z}(t) \\ \Im \vec{Z}(t) \end{bmatrix} \Big| \vec{W}(t) \sim \mathcal{N} \left(\begin{bmatrix} \cos \vec{\Phi}(t, \vec{W}) \\ \sin \vec{\Phi}(t, \vec{W}) \end{bmatrix}, I \frac{\sigma_n^2}{2} \right). \quad (5)$$

For simplicity, the three random position components of $\vec{W}(t)$ are assumed to be independent of one another. Then, their contribution to the phase is a scalar Gaussian random variable:

$$\vec{\Phi}(t, \vec{W}) = \frac{4\pi f}{c} (\hat{p}(t)^T \vec{r}_0 + \underbrace{\hat{p}(t)^T \vec{W}(t)}_{W_p(t)})$$

The one-dimensional random range offset at time t , $W_p(t) \sim \mathcal{N}(0, \hat{p}(t)^T \text{Cov}(\vec{W}(t)) \hat{p}(t))$. Here, $\vec{r}_0 = [x_0, y_0, z_0]^T$.

Note that these two Gaussian densities are separately easy to work with, so we can use numerical techniques to obtain the joint log-likelihood of Monte Carlo-generated observations, and then their Hessians (matrix of double derivatives). Averaged over many such Monte Carlo trials, negative Hessians would yield an estimate for the FIM that converges to the true FIM as the number of samples grows large.

Specifically, marginalizing (5) over $W_p(t)$, which we treat as a scalar variable,

$$P \left(\begin{bmatrix} \Re \vec{Z}(t) \\ \Im \vec{Z}(t) \end{bmatrix} \right) = \int_{-\infty}^{\infty} P \left(\begin{bmatrix} \Re \vec{Z}(t) \\ \Im \vec{Z}(t) \end{bmatrix} \Big| W_p(t) \right) \mathcal{N} \left(W_p(t); 0, \hat{p}(t)^T \text{Cov}(\vec{W}(t)) \hat{p}(t) \right) dW_p(t), \quad (6)$$

where $\mathcal{N}(z; \mu, \sigma^2)$ evaluates the Gaussian density with mean μ and variance σ^2 at z . This integral can be evaluated numerically, for example with Matlab's "quadgk()" function. For uncorrelated random motion, the joint log-likelihood of all observations, $\underline{Z} = [\vec{Z}(t_1)^T, \dots, \vec{Z}(t_{N_\phi})^T]^T$, is a sum over all these *log-marginals*:

$$\log P(\underline{Z}) = \sum_t \log P \left(\begin{bmatrix} \Re \vec{Z}(t) \\ \Im \vec{Z}(t) \end{bmatrix} \right). \quad (7)$$

Recall that the observations' joint log-likelihood is the first step in evaluating the FIM. We generate Monte Carlo samples of \underline{Z} ; for each such sample, we compute its log-likelihood, numerically twice-differentiate it over $\Theta = [|a|, \angle a, x_0, y_0, z_0, v_x, v_y, v_z]^T$, and obtain a sample of the negative FIM. Averaging over several such samples gives an estimate of the true FIM, which can be inverted to obtain the CRB matrix.

B. Linearized CRB

Correlated motion would require higher-order numerical integration of (6) since $W_p(t)$ pulse-to-pulse are not independent. Although this integration could be accomplished by MCMC methods, an alternative approach is to approximate the data model with a first-order Taylor series about $E[\vec{\Phi}(t)]$:

$$\begin{aligned}\vec{Z}(t) &= a \exp(j\vec{\Phi}(t)) + \vec{n}_Z(t) \\ &\approx a \exp(jE[\vec{\Phi}(t)]) \left(1 + j\vec{\Phi}(t) - jE[\vec{\Phi}(t)]\right) + \vec{n}_Z(t) \\ &= \vec{Z}_{lin}(t).\end{aligned}\quad (8)$$

This approximation is valid if

$$\frac{1}{2}(\vec{\Phi}(t) - E[\vec{\Phi}(t)])^2 \ll \vec{\Phi}(t) - E[\vec{\Phi}(t)] \quad (9)$$

for all elements in $\vec{\Phi}(t)$.

With this approximation, the complete data vector \underline{Z}_{lin} becomes a jointly Gaussian random vector. The Slepian-Bangs formulation gives the Cramér-Rao bound under jointly Gaussian random vectors [9, Appendix B]. However, a small extension is required for complex random vectors that are not circular, that is, where for a complex random vector \vec{z} ,¹

$$E[(z - E[\vec{z}])(z - E[\vec{z}])^T] \neq 0.$$

For non-circular complex random vectors, it can be shown [10] that the CRB is given as follows. Consider an n -variate complex Gaussian random vector $\vec{z} = \vec{x} + j\vec{y}$ with mean $\vec{m}_z = E[\vec{x}] + jE[\vec{y}] = \vec{m}_x + j\vec{m}_y$, covariance $\mathbf{R}_z = E[(\vec{z} - \vec{m}_z)(\vec{z} - \vec{m}_z)^H]$, and what Picinbono calls the *relation matrix*, $\mathbf{R}'_z = E[(\vec{z} - \vec{m}_z)(\vec{z} - \vec{m}_z)^T]$.

The mean and the covariance and relation matrices are parameterized by a vector of unknowns $\Theta \in \mathcal{R}^L$, and each element of the $L \times L$ Fisher information matrix F is given by

$$F_{ij} = \frac{1}{2} \text{tr} \left[\partial_i \tilde{\mathbf{R}} \tilde{\mathbf{R}}^{-1} \partial_j \tilde{\mathbf{R}} \tilde{\mathbf{R}}^{-1} \right] + (\partial_i \mathbf{m})^H \tilde{\mathbf{R}}^{-1} (\partial_j \mathbf{m}) \quad (10)$$

with $\mathbf{m} = \begin{bmatrix} \vec{m}_z \\ \vec{m}_z^* \end{bmatrix}$ and $\tilde{\mathbf{R}} = \begin{bmatrix} \mathbf{R}_z & \mathbf{R}'_z \\ \mathbf{R}'_z^* & \mathbf{R}_z^* \end{bmatrix}$. We have used $\partial_i \mathbf{A} \equiv \frac{\partial \mathbf{A}}{\partial \Theta_i}$ for $\Theta_i \in \Theta$ and any vector or matrix \mathbf{A} .

We now apply the extended Slepian-Bangs formula to the present data model. A notational convenience: let an underbar denote the $N_f N_\phi \times 1$ vector formed by rasterizing any variable's values over the complete $N_f \times N_\phi$ data collection, similar to \underline{Z} above.

\underline{Z}_{lin} is fully described by its mean vector, and covariance and relation ($E[(\underline{Z} - E[\underline{Z}])(\underline{Z} - E[\underline{Z}])^T]$) matrices. First,

$$E[\underline{Z}] = E[\underline{Z}_{lin}] = a \exp(jE[\underline{\Phi}]). \quad (11)$$

The covariance matrix \mathbf{R} is

$$\begin{aligned}\mathbf{R} &= \text{Cov}(\underline{Z}_{lin}) = \text{Cov}(jE[\underline{Z}] \odot \underline{\Phi}) + I\sigma_n^2 \\ &= \text{Cov}(\underbrace{\text{diag}(jE[\underline{Z}]) \cdot \underline{\Phi}}_{\mathbf{D}}) + I\sigma_n^2 \\ &= \mathbf{D} \text{Cov}(\underline{\Phi}) \mathbf{D}^H + I\sigma_n^2.\end{aligned}\quad (12)$$

¹We will use $()^T$, $()^H$, $()^*$, and \odot to mean transpose, conjugate transpose, complex conjugate, and the element-wise Hadamard product, respectively.

Only \mathbf{D} is a function of the unknowns Θ . The randomness in $\underline{\Phi}$ is due to

$$\underline{W}_x = [\bar{\mathbf{I}}_{N_f}^T W_x(t_1), \dots, \bar{\mathbf{I}}_{N_f}^T W_x(t_{N_\phi})]^T$$

as well as \underline{W}_y and \underline{W}_z : note that each time instance's random variables are replicated N_f times. Therefore,

$$\begin{aligned}\text{Cov}(\underline{\Phi}) &= \text{Cov}(\text{diag}(\underline{k}_x) \underline{W}_x + \text{diag}(\underline{k}_y) \underline{W}_y + \text{diag}(\underline{k}_z) \underline{W}_z) \\ &= \sum_{\square \in \{x,y,z\}} \text{diag}(\underline{k}_\square) \text{Cov}(\underline{W}_\square) \text{diag}(\underline{k}_\square)\end{aligned}\quad (13)$$

where the second line follows if we assume that the three random motion processes are independent of one another, and where each scalar element of the observed data vector is associated with a coordinate in Fourier space $[k_x, k_y, k_z] = \frac{4\pi}{c} f [\cos \theta \sin \phi, \cos \theta \cos \phi, \sin \theta]$, for the azimuth and elevation angles ϕ and θ corresponding to that phase history point. $\text{Cov}(\underline{W}_y)$ and $\text{Cov}(\underline{W}_z)$ are specified in the same manner as $\text{Cov}(\underline{W}_x)$:

$$\text{Cov}(\underline{W}_x) = \text{Expand}(\text{Toeplitz}(\vec{r}_{W_x}), N_f) \quad (14)$$

where $\vec{r}_{W_x} = [r_{W_x}(0), \dots, r_{W_x}(N_\phi - 1)]^T$ for autocorrelation sequence $r_{W_x}(\tau)$. The function $\text{Expand}(\mathbf{A}, m)$ yields a square matrix where each element of matrix \mathbf{A} has been replicated m times vertically and horizontally: this addresses the fact that the random motion at each pulse is replicated in N_f observations. $\text{Toeplitz}(\vec{r}_{W_x})$ yields the $N_\phi \times N_\phi$ Toeplitz matrix made from vector \vec{r}_{W_x} , with constant values corresponding to the elements of \vec{r}_{W_x} along the negative-sloping diagonals [9, Appendix A].

The derivation of the relation matrix, \mathbf{R}' , follows similarly and yields

$$\mathbf{R}' = \mathbf{D} \text{Cov}(\underline{\Phi}) \mathbf{D}. \quad (15)$$

The derivatives of the mean vector and covariance-relation matrix pair are all parameterized by the derivatives of $\mathbf{D} = \text{diag}(jE[\underline{Z}])$:

$$\partial_i \mathbf{D} = j \text{diag}(\partial_i E[\underline{Z}]), \quad (16)$$

for

$$\partial_i E[\underline{Z}] = \begin{cases} j \underline{k}_x \odot E[\underline{Z}] & \Theta_i = x_0 \\ j \underline{k}_y \odot E[\underline{Z}] & \Theta_i = y_0 \\ j \underline{k}_z \odot E[\underline{Z}] & \Theta_i = z_0 \\ j \underline{t} \odot \underline{k}_x \odot E[\underline{Z}] & \Theta_i = v_x \\ j \underline{t} \odot \underline{k}_y \odot E[\underline{Z}] & \Theta_i = v_y \\ j \underline{t} \odot \underline{k}_z \odot E[\underline{Z}] & \Theta_i = v_z \\ \frac{1}{|a|} E[\underline{Z}] & \Theta_i = |a| \\ j E[\underline{Z}] & \Theta_i = \angle a. \end{cases} \quad (17)$$

Equations (10) through (17) complete the specification of the FIM for the linearized model. We use this approximation as well as the full Monte Carlo approximation in (6)-(7) to evaluate CRBs and quantify the impact of random motion on target focusing.

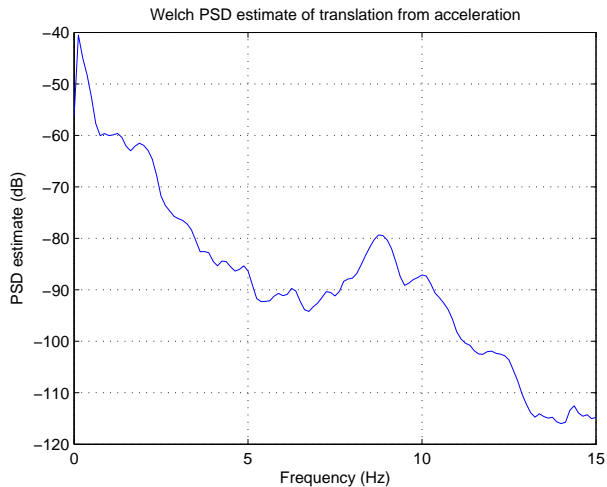


Fig. 1. PSD estimate from 20 seconds of accelerometer data for a driving Chevrolet Suburban, with a fifteen-order polynomial trend removed. -60 dB corresponds to amplitudes of 1 mm (the plateau at 1-2 Hz), and -80 dB to 0.1 mm (the small peak at 8.75 Hz). Data courtesy of OSU Center for Mapping.

IV. IMPACT OF RANDOM MOTION ON LOCALIZATION

In [5], an elegant CRB formulation was given for scatterer amplitude and location under no motion. This serves as a baseline for comparison to estimation error with our current motion model. This is also motivation to consider estimating *position only*. Another reason for this is that when target velocity is unknown and must be estimated, ambiguities are introduced into position estimation, ambiguities which would be much better described by a more sophisticated target model.²

For both these reasons, we consider scatterer localization performance only. We seek to understand the degradation of location estimation accuracy caused by random motion. With this goal in mind, we furthermore consider only *two-dimensional localization*, of x_0 and y_0 , and treat height, z_0 , to be known. There is no computational reason that z -estimation cannot be considered but in [5], it was observed that for single-pass SAR images, off-plane height estimation is very poor over short apertures and *does improve as a target's angular persistence increases*. Because we seek to understand degradations due to random motion alone, minimizing the role of such effects is justified.

For these reasons, our vector of unknowns is $\Theta = [a, \angle a, x_0, y_0]$ for a single point scatterer vibrating in a two-dimensional horizontal plane. Assuming a SAR imaging at 10 GHz with 650 MHz bandwidth, a circular flightpath at elevation angle of 45° and standoff distance of 8.5 km, we consider the effects of two main motion parameters:

- σ_x and σ_y : the standard deviation of the motion random processes, and

²Specifically, when down-range velocity v_y is unknown, the CRB error on cross-range position x_0 immediately explodes to the entire illuminated scene width. This is understandable because a target with down-range velocity has phase history very similar to a stationary target displaced in cross-range. Ongoing research on a collection-of-reflectors target would describe within-target reflector localization without this ambiguity.

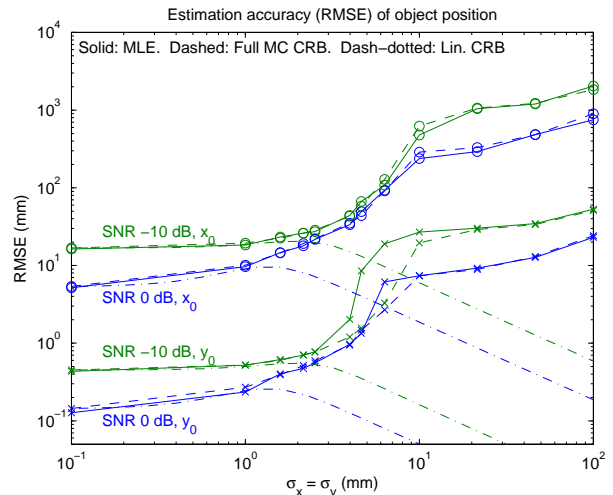


Fig. 2. Estimating down-range and cross-range positions, y_0 and x_0 . Maximum likelihood estimator (MLE) standard deviations, and root mean squared errors (RMSE) for both the unapproximated Monte Carlo CRB and the linearized CRB at two SNRs. Note that both axes are on the log scale, and in units of millimeters.

- the spectral content of these random motion processes.

Preliminary study (Figure 1) of inertial measurement unit (IMU) data gives reason to believe that translational motion of an SUV is approximately a low-pass signal. The PSD estimate is from a 20 second time segment and is representative of motion in all dimensions. In keeping with the goal of obtaining simple insights into the effects of random motion, we treat the motion random processes to be white noise passed through ideal low-pass filters with varying cutoff frequency, ω_c .

A. Uncorrelated motion

First, we consider uncorrelated two-dimensional motion. Figure 2 shows the behavior of both CRB-predicted estimation errors for cross- and down-range position x_0 and y_0 , as well as the standard deviation of a maximum likelihood estimator (MLE), implemented as a nonlinear function maximization using “fminsearch()” in Matlab. Both the Monte Carlo CRB and the MLE were obtained for 250 Monte Carlo iterations. The imaging aperture was held constant at 5° , and for computational reasons, the ground patch was very small (5 m diameter).

1) *Full Monte Carlo CRB trends*: We begin by observing that the predicted estimation error of the full CRB (obtained by numerical techniques) is tracked closely by the MLE. Two separate regimes make themselves apparent: for low-power random motion, $\sigma_x, \sigma_y < 1$ mm, localization error is dominated by sensor noise, with motion playing a relatively small role. After a transition, the roles are reversed as uncertainty due to random motion dominates.

In this motion-dominated regime, localization error in both downrange and cross-range can be increase to *two orders of magnitude greater* than the no-motion regime.

2) *Differences between localizing in down-range vs. cross-range*: The radar literature, e.g., [6], observes that localization in down-range is much more accurate than in cross-range,

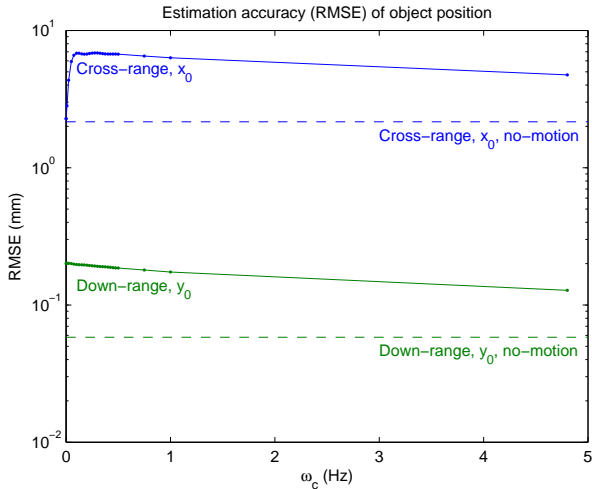


Fig. 3. Estimating down-range and cross-range location, y_0 and x_0 : linearized CRB-predicted RMSE for correlated random motion, at fixed $\sigma_x = \sigma_y = 1$ mm, for a 10 m scene diameter at 0 dB SNR. Uncorrelated motion corresponds to the right-most point. The no-motion baseline is also shown: the cross-range and down-range curves peaks at 3.1 times and 3.4 times their respective baselines.

and that cross-range resolution is a function of angular extent (which is 5° in this example). This is reflected in Figure 2 by the large gap between each curve of the same SNR. Figure 2 additionally shows that given this difference, similar degradation occurs in both down- and cross-range.

3) *Behavior of linearized CRB*: As expected, the linearized CRB in Figure 2 closely approximates the Monte Carlo-generated CRB for low motion error, when the linear approximation in (9) is valid. However, the approximation has broken down at motion standard deviation of 1 mm (applying (9) at two standard deviations, the quadratic term, $\frac{1}{2}(0.002\frac{4\pi f_c}{c})^2$, is 20% of the linear term). The linearized CRB curves beyond $\sigma_x = \sigma_y = 1$ mm are not accurate approximations of the true CRB.

B. Correlated motion

To consider the effects of correlated (non-white) random motion, the linearized CRB for ideal low-pass filtered motion with varying cutoff frequencies, ω_c is given in Figure 3, with a motion-free CRB-predicted baseline also shown. For this analysis, motion standard deviations $\sigma_x = \sigma_y$ were fixed to 1 mm, and this motion power was preserved across all cutoff frequencies—that is, random motion is generated by passing white noise with standard deviation of 1 mm into a low-pass filter with cutoff ω_c and amplitude of $\omega_c/(PRF/2)$. Here, we consider a somewhat larger scene size with 10 m diameter, and the same 5° aperture and 0 dB SNR as before.

From Figure 3 we see that to a first-order approximation, changing spectral content does *not* significantly impact target localization. That is, once a target has a given random vibration power, which frequencies such vibration manifests itself is largely immaterial to localization error.

Two other observations are worth noting. First, random motion that is uncorrelated is more benevolent than highly-correlated motion, for both cross- and down-range. This is to be expected, especially since 1 mm motion standard deviations do not cause wrapping of the phase $\underline{\Phi}$, because extracting underlying parameters is “easier” in uncorrelated observations than in correlated ones. Secondly, highly-correlated motion induces very little increase in crossrange estimation error, but this error quickly rises as the motion spectral diversity increases. The analogy we use to understand this is, using the small-angle approximations for $\hat{p}(t)$ (the unit vector pointing from scene center to the radar at time t), estimating a target’s down-range position y_0 is akin to estimating the intercept of a line, while estimating its cross-range position x_0 is like estimating its slope. As motion introduces “noise” that is much stronger in the down-range dimension, cross-range (slope) estimation suffers much less from fully-correlated motion than down-range (intercept) estimation.

V. CONCLUSION

Motivated by evaluating performance of moving target focusing algorithms, we have obtained Cramér-Rao bounds for estimating the position and velocity of a single point scatterer moving with non-zero velocity and some random motion component. We use these bounds to show that when point scatterers have even a minute amount of random jitter, with standard deviation in the centimeters, localization error can increase by two orders of magnitude above the motion-free case. We also show that the spectral content of this noise does not significantly affect this degradation in localization.

REFERENCES

- [1] J. Jao, “Theory of synthetic aperture radar imaging of a moving target,” *Geoscience and Remote Sensing, IEEE Transactions on*, vol. 39, pp. 1984–1992, Sept. 2001.
- [2] S. Scarborough, C. Lemanski, H. Nichols, G. Owirka, M. Minardi, and T. Hale, “SAR change detection MTI,” in *Algorithms for Synthetic Aperture Radar Imagery XIII*, May 2006.
- [3] B. Rigling, “Multistage entropy minimization for SAR image autofocus,” in *Algorithms for Synthetic Aperture Radar Imagery XII*, May 2006.
- [4] D. Wahl, P. Eichel, D. Ghiglia, and C. Jakowatz, “Phase gradient autofocus—a robust tool for high resolution SAR phase correction,” *Aerospace and Electronic Systems, IEEE Transactions on*, vol. 30, pp. 827–835, Jul 1994.
- [5] L. Moore and L. Potter, “Three-dimensional resolution in circular synthetic aperture radar,” *submitted to IEEE Transactions on Image Processing*, August 2007.
- [6] C. Jakowatz, D. Wahl, P. Eichel, and D. Ghiglia, *Spotlight-Mode Synthetic Aperture Radar: A Signal Processing Approach*. New York: Springer, 1996.
- [7] B. Rigling, “Analysis of target rotation and translation in SAR imagery,” *to appear, Algorithms for Synthetic Aperture Radar Imagery XVI*, 2009.
- [8] B. P. Lathi, *Modern Digital and Analog Communication Systems*. New York: Oxford University Press, 1998.
- [9] P. Stoica and R. L. Moses, *Introduction to Spectral Analysis*. New Jersey: Prentice-Hall, 2005.
- [10] J.-P. Delmas and H. Abeida, “Stochastic Cramér-Rao bound for noncircular signals with application to DOA estimation,” *Signal Processing, IEEE Transactions on*, vol. 52, no. 11, pp. 3192–3199, Nov. 2004.
- [11] B. Picinbono, “Second-order complex random vectors and normal distributions,” *Signal Processing, IEEE Transactions on*, vol. 44, pp. 2637–2640, Oct 1996.